Journal of Power Sources 195 (2010) 7090–7097

Contents lists available at ScienceDirect

Journal of Power Sources

journal homepage: www.elsevier.com/locate/jpowsour

Low-temperature behavior of graphite–tin composite anodes for Li-ion batteries

F. Nobili*, M. Mancini, S. Dsoke, R. Tossici, R. Marassi

Scuola di Scienze e Tecnologie, Sezione Chimica, Università di Camerino, Via S. Agostino, 1, I-62032 Camerino (MC), Italy

ARTICLE INFO

Article history:
Received 22 January 2010
Received in revised form 27 April 2010
Accepted 1 May 2010
Available online 7 May 2010

Keywords:
Li-ion batteries
Graphite anodes
Sn composites
Intercalation kinetics
Electrochemical impedance spectroscopy

ABSTRACT

The challenge of increasing low-temperature performances of anodes for Li-ion batteries is faced by preparing graphite–tin composite electrodes. The anodes are prepared by mixing partially oxidized graphite with nanometric Sn powder or by coating the oxidized graphite electrode with a thin Sn layer. Long-term cycling stability and intercalation/deintercalation performances of the composite anodes in the temperature range 20 °C to −30 °C are evaluated. Kinetics is investigated by cyclic voltammetry and electrochemical impedance spectroscopy, in the attempt to explain the role of Sn in reducing the overall electrode polarization at low temperature. Two possible mechanisms of action for bulk metal powder and surface metal layer are proposed.

1. Introduction

Since the introduction of Li-ion batteries in the market, graphite has been the most used anodic material, due to the relatively flat charge/discharge profiles, with potentials quite close to the one of metal Li, the relatively high reversible capacity and the intrinsic safety of the material.

However, graphite anodes suffer from severe limitations when used at low temperature [1–4], mainly because of a high polarization during Li loading that forces the electrode to closely approach the Li deposition potential before the intercalation process is completed. This behavior can be ascribed to kinetic limitations, such as an activation polarization of the charge-transfer process, or to a reduced Li^+ ion solid-state diffusivity, as well as to an increase of the ohmic resistance of the active material, of the liquid electrolyte and of the passivation layer. All of these factors concur in producing an abrupt decrease of lithium intercalation capacity at temperatures below −20 °C. At −30 °C graphite totally loses its intercalation ability [5].

Mild oxidation of graphite, performed by thermal treatment, has been proven to be effective in enhancing performances and reducing irreversible capacity [6], while several electrolyte formulations have been investigated in order to improve the surface layer and the properties of Li^+ transport [7–10].

A practice commonly used to increase the anode intercalation ability is the preparation of metal–graphite composites, either by dispersing a metal powder in the formulation of the electrodes or by covering the electrodes surface with metal coatings [11–26]. In recent papers we investigated [5,27–29] the behavior of several composite anodes prepared with graphite and metals, both forming and not forming alloys with Li, such as Sn and Cu, respectively. The electrodes have been prepared by finely dispersing very low amounts (1%, w/o) of nanosized metallic powders (Ag, Al, Au, Cu, Ni, Sn) in the bulk of graphite or by coating the graphite anode surface with very thin (50 Å thick) metallic layers (Ag, Al, Au, Bi, Cu, In, Ni, Pb, Pd, Sn, Zn). Both preparation methodologies are relatively inexpensive and very easy to carry out. The same technique, therefore, can also been applied to the preparation of metal–graphite composites with higher metal loadings, potentially leading to composite electrodes in which both graphite and alloy-forming metal may reversibly exchange lithium and, at the same time, graphite may act as a buffer material to compensate for the volume expansion characteristic of metal alloy electrodes, without the use of expensive organic precursors as templates [30–37].

For all the electrodes an improvement of the cycling behavior has been demonstrated, with the only drawback of an increased irreversible capacity in the first cycle, due to formation of a solid electrolyte interface (SEI) that probably involves also the metals. Metal–graphite composite anodes prepared by mixing Cu, Sn or Al nanosized powders retain a remarkable intercalation ability even at −30 °C (up to 30% of the theoretical capacity) [5]. The same behavior has been observed for Cu-coated graphite electrodes. In this case the dependence of the electrochemical performances on the thickness of the coating has also been studied [28,29]. Recently, Cu or Sn coatings have been also successfully applied to improve the electrochemical behavior of anatase TiO_2 anodes [38,39].

* Corresponding author. Tel.: +39 0737402210; fax: +39 0737402296.
E-mail address: francesco.nobili@unicam.it (F. Nobili).

0378-7753/$ – see front matter © 2010 Elsevier B.V. All rights reserved.
doi:10.1016/j.jpowsour.2010.05.001

The intercalation kinetics of some metal–graphite composite anodes has been already investigated. A reduction of the charge-transfer and SEI resistances with respect to the unmodified electrodes has been found. For Cu–graphite composite electrodes an enhancement in charge-transfer kinetics has been demonstrated. This has been tentatively attributed to a catalytic effect of the metal on the Li^+ ion desolvation, that is known to be the rate-limiting step of the intercalation process [27,40–43].

In order to further validate this hypothesis in the case of a Li-alloy forming metal, this paper deals with the electrochemical characterization at several temperatures of the charge/discharge behavior and of the intercalation kinetics of Sn–graphite composite anodes, prepared either by dispersing the metallic powder in graphite or by coating the electrodes with a thin metallic layer. The evaluation of intercalation/deintercalation performances, already introduced in Refs. [5,28], is completed here for all the Sn–graphite anodes in the temperature range 20 °C to −30 °C. The investigation of kinetics is carried out by the analysis of impedance response of the electrodes in the same temperature range.

2. Experimental

Mild oxidation of graphite (Timrex KS-15 by Timcall, specific area 12 $m^2 g^{-1}$, average particle size 7.7 μm, interlayer distance 3.36 Å) has been carried out by thermal treatment at 750 °C for 45 min. Since the pristine graphite had been previously dried under vacuum at 200 °C, the oxidation degree could be roughly estimated by weight loss (about 25–30%) and by oxygen content (about 11%), as determined by elemental analysis.

Electrodes of oxidized graphite, used for comparison purposes (designated as A), were prepared using the "doctor blade" technique [5,27–29] that permits control of the loading. A slurry containing 84.5% oxidized graphite, 5% conductive carbon (Super-P by MMM Carbon), 10% binder (PVdF by Aldrich), 0.5% oxalic acid $H_2C_2O_4$ (Carlo Erba) (weight ratio) in NM2P (N-metyl-2-pyrrolidinone by Aldrich) was spread with a controlled thickness over a Cu foil current collector (12.5 μm thick by Schlenk). The oxalic acid in the slurry partially etches the Cu current collector by removing surface oxides, and thus improves graphite adhesion to the substrate. Unreacted acid decomposes during the drying step, that has been carried out at 75 °C in air atmosphere and then at 120 °C under vacuum.

Sn-coated anodes, designated as B, were prepared following the same procedure reported in Ref. [28]. A 50 Å thick Sn coating has been applied over type A electrodes by physical vapor deposition (PVD) in a vacuum chamber, using a tungsten crucible to hold pure Sn metal. The metal has been evaporated onto the graphite electrode, used as substrate and kept at room temperature, by applying suitable currents (about 100 Å) to the crucible. Deposit thickness has been monitored by a quartz crystal microbalance close to the electrode.

Anodes containing metal particles, designated as C, were prepared by following the same procedure reported in Ref. [5]. A dispersion of Sn powder (≤100 nm, Aldrich) in Super-P carbon (weight ratio carbon:Sn 80:20) has been prepared by mechanical stirring in Ar atmosphere. This dispersion was used instead of pure Super P as conductive agent in the slurry used to prepare the electrodes, to obtain a final metal content of about 1% (w/o).

The graphite loadings of all the electrodes A–C (0.64 cm^2 area) resulted in the range 2–3 mg cm^{-2}.

Electrode morphology was investigated using a Cambridge Stereoscan mod. 360 scanning electron microscope (SEM).

The electrochemical measurements were performed with T-shaped polypropylene Swagelok type cells, equipped with stainless steel (SS304) current collectors. Two polypropylene films (Celgard 2400, Celanese Co.) were used as separators. A solution of $LiPF_6$ 1 M in EC:DEC:DMC 1:1:1 (LP71 by Merck) was used as electrolyte. The ternary solvent system allows to avoid complications due to solvent freezing at low temperatures [10,44]. Metallic Li by Foote Mineral Co. has been used for counter and reference electrodes. The reference electrode has been assembled as a Li strip supported on a stainless steel grid interposed between two Celgard disks and placed between counter and working electrodes. This arrangement is crucial in improving the quality of electrochemical impedance spectroscopy measurements. The cells were assembled in a glove box under Ar atmosphere with O_2 and H_2O contents below 10 ppm and cycled 3 times at C/3 rate in order to allow a complete and homogeneous formation of solid electrolyte interface (SEI) over the surface of the electrodes. The cells were successively opened in order to eliminate any possible gases developed during SEI formation, sealed again and brought out of the box to complete the electrochemical investigations. Temperature was regulated by holding the cells in a programmable freezer in which the temperature was controlled within ±1 °C.

The cells were continuously cycled between 0.01 V and 1.5 V, at a C/5 charge/discharge rate and in the temperature range 20 °C to −30 °C. Slow scan rate cyclic voltammetries (SSCV) were performed in the potential range 0.01–0.3 V at 0.01 mV s^{-1}. The electrochemical impedance spectra (EIS) were acquired in the frequency range 1 mHz to 100 kHz with a sinusoidal perturbation of 5 mV applied over the bias potential.

All the electrochemical measurements have been performed using a VMP2/Z multi-channel galvanostat–potentiostat by PAR Instruments (Oak Ridge, TN). For sake of comparison, all the results obtained have been normalized to the actual active masses of the electrodes. All the potentials are given vs Li^+/Li.

3. Results and discussion

3.1. Morphology

Morphology of the electrodes has been investigated by scanning electrode microscopy (SEM). The micrographs of electrodes A and B have already been shown in Ref. [27]. The secondary electrons image of electrode C (Fig. 1a) reveals that the average size of graphite grains is of the order of few micrometers, as for the other anodes investigated. The backscattered electrons image (Fig. 1b) reveals that most of the dispersed Sn powder is still at nanosize level, even if few micrometric aggregates are present.

3.2. Galvanostatic measurements

Galvanostatic cycles have been performed in order to evaluate cycling stability of the electrodes and to compare reversible and irreversible capacity. The trends of intercalation capacity are shown in Fig. 2 and relevant values at selected cycles are listed in Table 1. For both Sn–graphite composites, the irreversible capacity is of the order of 180–200 mAh g^{-1}. These quite high values are common for this class of electrodes [5,27–29], and can be ascribed to alternative/additional processes of SEI formation involving the metal, that provides a further surface at which electrolyte reactions can be catalyzed. This is in agreement with the results obtained, for instance, by Hassoun et al. [45], who propose an active role of Sn surface in catalyzing electrolyte decomposition.

The reversible intercalation capacity is practically constant after 40 cycles, revealing a good cycling stability. The values obtained for type B electrodes are, within an experimental error of few mAh g^{-1}, in good agreement with those published in Ref. [28] referring to the deintercalation step.

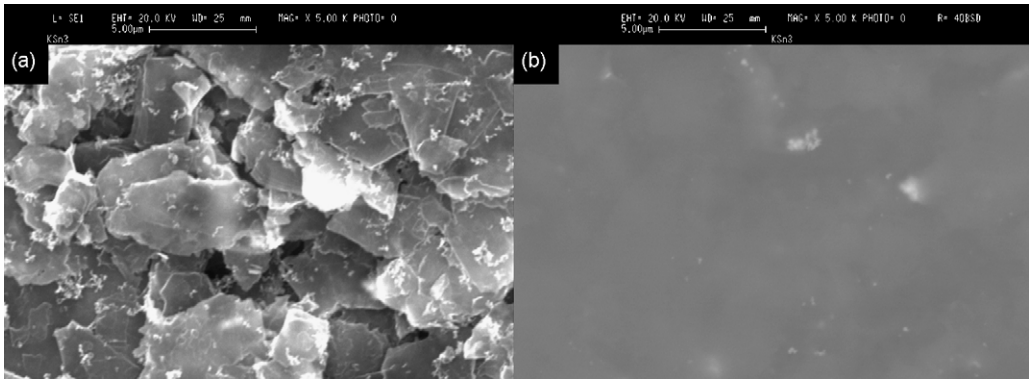

Fig. 1. SEM images of composite anode (C), containing 1% Sn dispersed in the bulk of graphite. Secondary electrons micrograph (a), backscattered electrons micrograph (b).

Table 1
Capacity values obtained during intercalation and deintercalation at selected cycles (first and second cycles at C/3 rate, twentieth cycle at C/5 rate). Values for electrode A from Ref. [27].

Electrode	Experimental capacity (mAh g^{-1})						
	1st int. C/3	1st deint. C/3	1st irrev. C/3	2nd int. C/3	2nd deint. C/3	20th int. C/5	20th deint. C/5
A	440	356	84	376	353	353	352
B	541	362	179	392	365	374	361
C	556	361	195	379	355	371	348

The cycling behavior as a function of temperature has been evaluated at C/5 rate in the range 20 to −30 °C. Both charge and discharge steps are limited by the amount of Li than can be inserted during the intercalation, that is the only process substantially affected by the low temperature conditions [5]. As a consequence, the reversible capacity can be estimated as a mean of the values obtained during intercalation and deintercalation steps. The obtained results are shown in Fig. 3. The electrochemical behavior of all the electrodes is similar down to 0 °C, while at lower temperatures electrode B, coated by a 50 Å thick Sn layer, shows better performances. At −20 °C also electrode C, containing 1% Sn powder dispersed in the bulk, shows a higher capacity than the pristine oxidized graphite electrode A. At −30 °C both electrodes B and C still show remarkable capacities (152 mAh g^{-1} and 94 mAh g^{-1}, respectively), while electrode A is practically unable to exchange any useful amount of Li$^+$. Table 2 reports the average capacity values at each temperature of the three electrodes under investigation. The values for electrode C closely resemble those published in Ref.

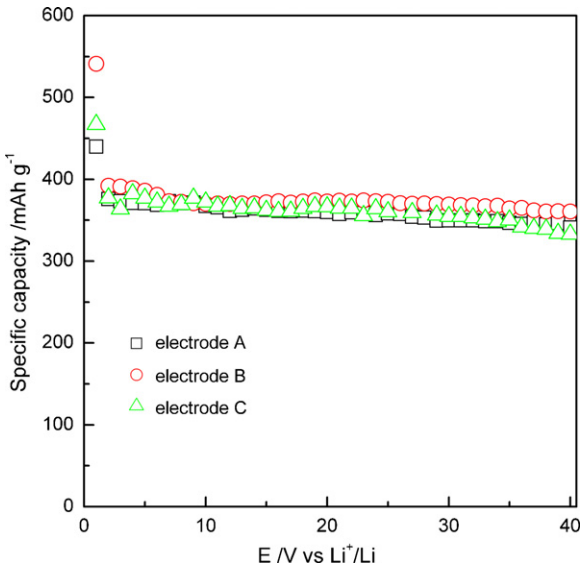

Fig. 2. Specific capacity values obtained during intercalation of Li$^+$ into pristine oxidized graphite anode (A), composite anode coated by a 50 Å Sn layer (B), composite anode containing 1% (w/o) Sn powder in the bulk of formulation (C). First 3 cycles run at C/3, the following at C/5 charge–discharge rate, T = 20 °C.

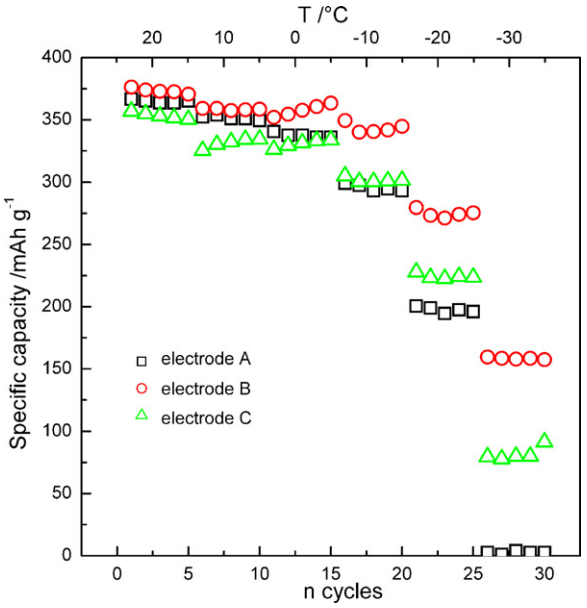

Fig. 3. Reversible capacity calculated as a mean value of intercalation and deintercalation processes, for electrodes A–C in the temperature range 20 °C to −30 °C.

Table 2
Reversible capacity values for electrodes A–C in the temperature range 20 °C to −30 °C. Values averaged among 5 galvanostatic cycles run continuously at C/5 rate.

	Reversible capacity (mAh g^{-1})					
Temperature (°C)	20	10	0	−10	−20	−30
Electrode						
A	365	351	339	296	196	1
B	377	360	357	342	273	152
C	370	365	339	299	226	94

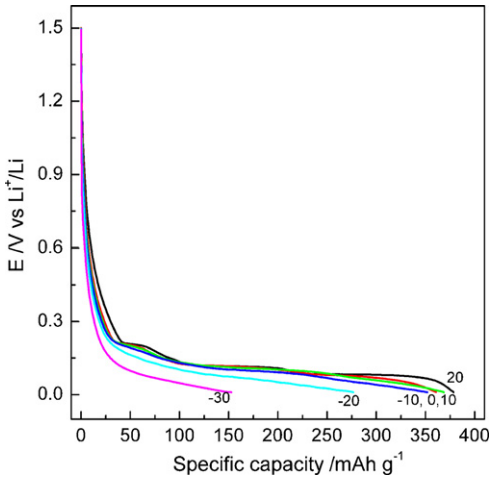

Fig. 4. Intercalation profiles of Sn–graphite composite anode B recorded at C/5 rate in the temperature range 20 °C to −30 °C.

[5], with only marginal differences at temperatures below 0 °C due to the lack of a potentiostatic top-off step. The intercalation curves at different temperatures for electrode B are shown in Fig. 4. In Fig. 5 the corresponding dQ/dE vs E profiles are reported, showing that at least one Li-graphite stage is formed even at the low temperature limit. This behavior is similar to the one observed for Sn powder–graphite electrode C reported in Ref. [5].

It should be noted that the very small amounts of Sn introduced in both anodes B and C (Sn loadings never exceed 1%, w/o) have no practical effect on the overall capacity of the electrodes. As a consequence, it is quite difficult, from the inspection of galvanostatic cycles and of the corresponding dQ/dE profiles, to detect features of eventual Li–Sn phases.

However, the differential capacity curves of type B electrodes prepared with thicker Sn deposits show in the range 0.3–1 V peaks pertaining to several Li–Sn alloying/dealloying processes [54]. The associated capacities, much lower than that of graphite because of the relatively low amount of metal, are retained during repeated cycles. This demonstrates two important facts: (1) the intercalation process, at least at coated electrodes, involves Li–Sn alloys formation and (2) the expansion-contraction processes that cause the rapid capacity losses do not appear to be important in the present case, probably because of the low amount of metal involved.

3.3. Cyclic voltammetry (CV)

In order to investigate the reasons of the improved intercalation capacity at low temperature, the different electrodes have been studied using low scan rate cyclic voltammetry.

Fig. 6 shows the voltammogram of the Sn powder-graphite composite anode C, compared to those of pristine oxidized graphite and Sn-coated electrodes A and B as taken from Ref. [28].

For all the electrodes the values of the intercalated charge, as calculated by integration of the voltammograms, are close to the theoretical one of 372 mAh g^{-1}. The shape of the voltammograms and the mid-point potentials (Ep_{mean} in Table 3) of the three main processes (LiC_6/LiC_{12}, LiC_{12}/LiC_{27}, LiC_{36}/LiC_{72}) are similar for all the electrodes and close to the ones expected for graphite (85 mV, 120 mV, 210 mV, respectively). This confirms that low amounts of Sn (1% for electrode C, less than 1% for coated electrode B) do not modify the thermodynamics of graphite intercalation compounds (GICs) formation.

Nevertheless, some differences in the kinetics of the processes are evidenced by different widths and resolutions of the corresponding peaks, and by different separations ($Ep_{an} - Ep_{cath}$ in Table 3) between the anodic and cathodic potentials. Every peaks of the electrodes B and C are sharper and with a lower separation between cathodic and anodic potentials than for electrode A. For instance, for the LiC_6/LiC_{12} process, the peak separation is 58 mV for electrode A, 28 mV for electrode B, 40 mV for electrode C. The same trend holds for the other processes. This indicates that the overall kinetics of the intercalation/deintercalation processes is better in the composite electrodes.

3.4. Electrochemical impedance spectroscopy (EIS)

The nature of the kinetic improvement has been investigated at various temperatures by electrochemical impedance spectroscopy. The EIS dispersions have been recorded at selected potentials in the range 0.25–0.05 V, in the temperature range 20 °C to −30 °C. At any potential or temperature variations, the electrodes have been equilibrated at the selected bias potentials for several hours, in order to ensure reproducible intercalation levels.

Fig. 7 shows the Nyquist plots recorded for the anodes A–C at 0.09 V, corresponding to the potential of LiC_6 formation, in the temperature range analyzed. The impedance dispersions of electrode A are in agreement with those reported in Ref. [27]. Some characteristic frequencies, representative for pristine and Sn–graphite composite anodes, respectively, are reported in panels (a) and (b). The dispersions are translated along Z'' axis for sake of clarity.

The most relevant feature of the dispersions is a middle-frequency semicircle that describes the rate-determining step of the overall intercalation process, i.e. the charge-transfer at the electrode/electrolyte interface. A partly overlapped semicircle at higher frequencies, more pronounced at lower temperatures, describes the accumulation of charge at the surface of SEI. At lower frequencies, a 45° dispersion followed by a vertical line describes diffusion towards a blocking electrode.

The comparison of Nyquist plots reveals that, at every temperature, the overall impedance, and particularly the middle-frequency semicircles, are about one order of magnitude lower for Sn-modified electrodes than for pristine graphite. In addition, the middle-frequency semicircle is the feature most affected by the temperature decrease. For all electrodes the diameter of the semicircle increases up to about two orders of magnitude when the temperature is lowered down to −30 °C.

The EIS data have been analyzed with the equivalent circuit method [46]. The experimental dispersions have been fitted with a circuit commonly used to simulate the behavior of intercalation electrodes [27–29,47–50]. In Boukamp's notation [51], the equivalent circuit may be written as $R_{el}(R_{SEI}C_{SEI})(R_{ct}C_{dl})WC_i$, where R_{el} is the resistance of the electrolyte, R_{SEI} and C_{SEI} are the resistance and the capacitance of the passivation layer, R_{ct} and C_{dl} are the charge-transfer resistance and the capacitance of the associated electrical double layer at electrode/electrolyte interface, W is the Warburg impedance that describes Li^+ diffusion and C_i is the differential intercalation capacity. In the fitting procedure C and W elements have been replaced with constant phase elements Q, in order to take in account any deviations from ideal behavior of the electrodes, due to heterogeneity or roughness [52]. The circuit is shown in the inset in Fig. 7 panel (c).

All of the fits were obtained with a good agreement between experimental and simulated data, with χ^2 values of the order of $10^{-4}/10^{-5}$.

Fig. 8 shows the values of the SEI resistances for the electrodes A–C, obtained at 20 °C at the different potentials. Despite the poor quality of the high-frequency-region data, these values clearly show that the addition of Sn in the formulation of the electrodes , either as a dispersed powder or as a surface coating, leads to a

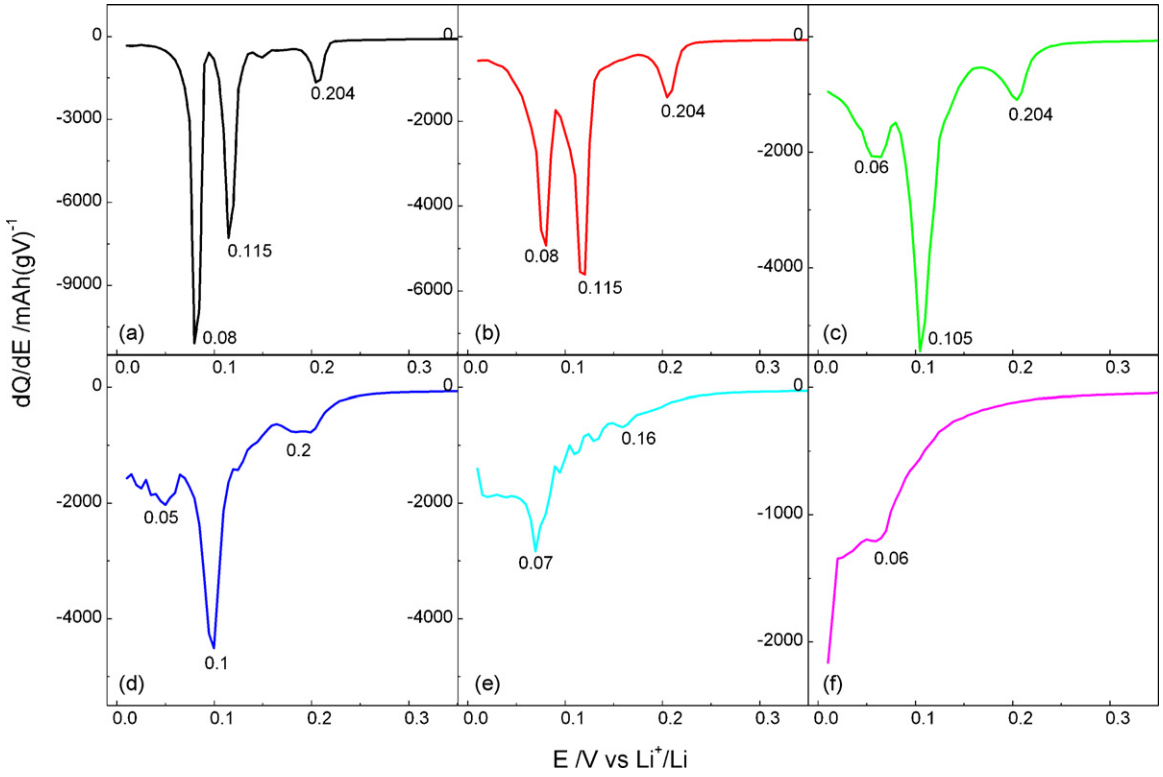

Fig. 5. Differential capacity dQ/dE vs E profiles of Sn–graphite composite anode B. (a) T = 20 °C, (b) T = 10 °C, (c) T = 0 °C, (d) T = −10 °C, (e) T = −20 °C, (f) T = −30 °C. Peak potentials (V) for stage formation processes are marked.

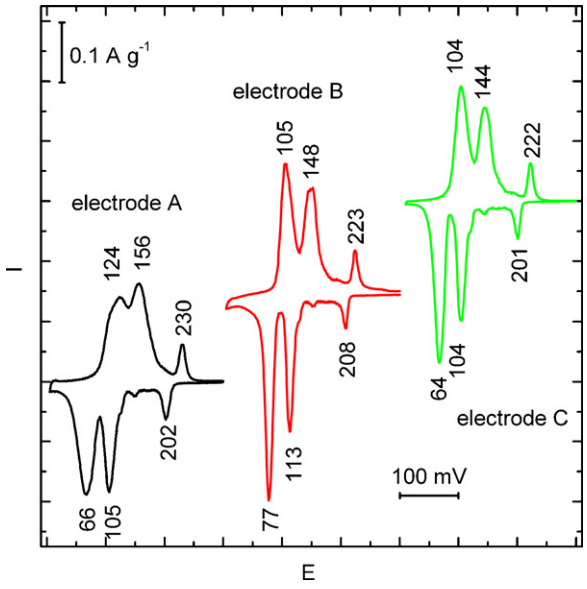

Fig. 6. Cyclic voltammograms of electrodes A–C recorded in the potential range 0.01–0.3 V at 0.01 mV s^{-1} scan rate. Peak potentials (mV) of main processes are marked. CV of electrodes A and B from Refs. [27,28], respectively, shown here for sake of comparison.

reduced resistance of the SEI. At any potential it is reasonable to expect that some of the metal, previously incorporated in SEI formation, is now part of the SEI structure presumably as some type of Li–Sn alloy.

Fig. 9a–c shows the calculated values of charge-transfer resistance at 20 °C, 0 °C and −30 °C. At all the temperatures, the R_{ct} values of Sn–graphite composites B and C are lower than those of electrode A, indicating a more facile electron transfer. At each temperature the values of R_{ct} are practically invariant with the potentials. This is in line with both old and recent findings and models for intercalation of Lithium into graphite, that attribute the so-called "charge-transfer" semicircle to a thermally activated process related to the rates of deintercalation of Li^+ ions and migration through the passivation layer. These two processes precede the Li^+ incorporation into the graphite lattice. As a consequence, the intercalation rate, that is directly proportional to $1/R_{ct}$, does not follow a classical Butler–Volmer type relationship with potential. This is known as the "adatom model" introduced by Bruce and Saidi [47], and extensively applied to intercalation electrodes [40–43,48–50].

The adatom model can also explain the reduction of R_{ct} observed for Sn–graphite composites. As already observed in the case of Cu–graphite composites [27–29], the reduction of R_{ct} can be ascribed to an active role of metal in enhancing the rate of desolvation of the adatom at electrode/electrolyte interface. This

Table 3
Mean values and separations between intercalation and deintercalation potentials of the three main voltammetric peaks (Ep_{mean}) for electrodes A–C.

Electrode	LiC_6/LiC_{12}		LiC_{12}/LiC_{27}		LiC_{36}/LiC_{72}	
	Ep_{mean} (mV)	$Ep_{an} - Ep_{cath}$ (mV)	Ep_{mean} (mV)	$Ep_{an} - Ep_{cath}$ (mV)	Ep_{mean} (mV)	$Ep_{an} - Ep_{cath}$ (mV)
A	95	58	130	51	216	28
B	91	28	131	35	216	15
C	84	40	124	40	212	21

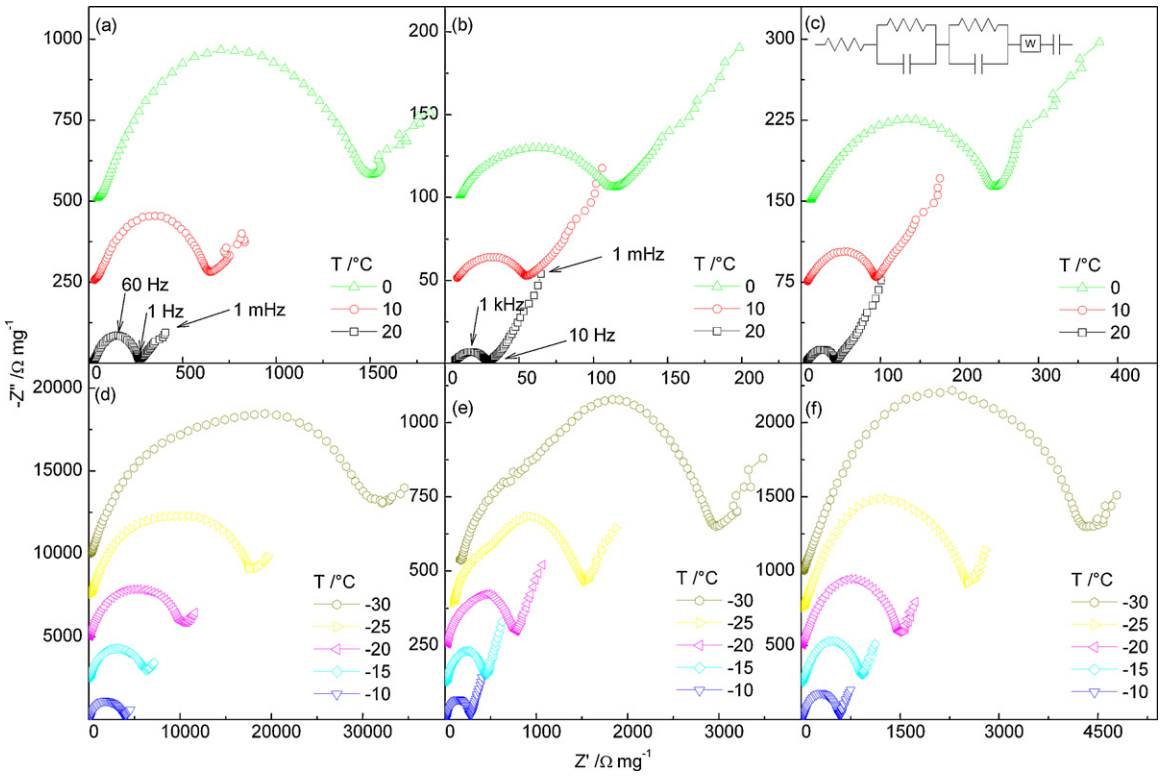

Fig. 7. Nyquist plots recorded in the temperature range 20 °C to −30 °C for electrodes A (panels a and d), B (panels b and e) and C (panels c and f), E = 0.09 V. Some characteristic frequencies in panel (a) for pristine oxidized graphite electrode and in panel (b) for Sn/graphite composites. Equivalent circuit in panel (c). Impedance data of electrode A from Ref. [27], shown here for sake of comparison.

interpretation is in agreement with Huang et al. [16], that showed a catalytic effect exerted by some metals or metallic oxides in accelerating Li^+ ion intercalation into graphite, either by enhancing the desolvation rate or by increasing the electron concentration at the electrode/electrolyte interface.

Since the intercalation is a thermally activated process, the dependence of R_{ct} on temperature can be described in terms of Arrhenius plots of the type

$$\frac{1}{R_{ct}} = A \exp\left(\frac{-E_a}{RT}\right) \quad (1)$$

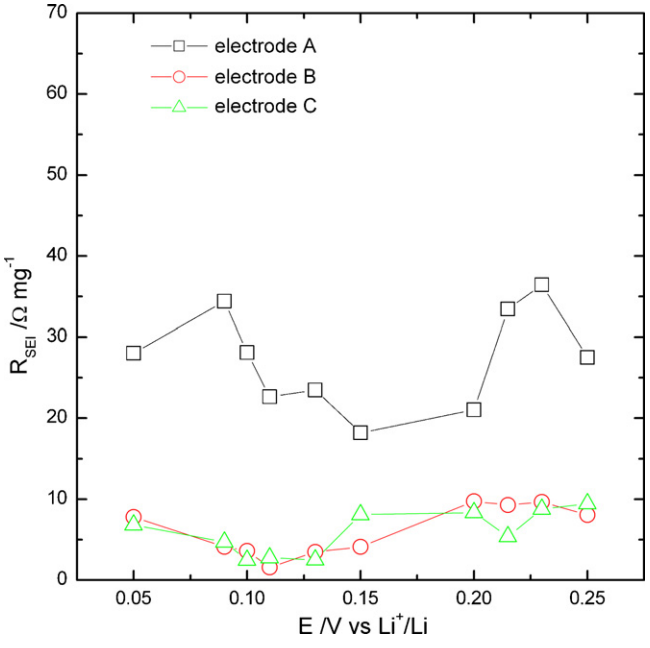

Fig. 8. Values of SEI resistances for electrodes A–C as a function of potential, T = 20 °C.

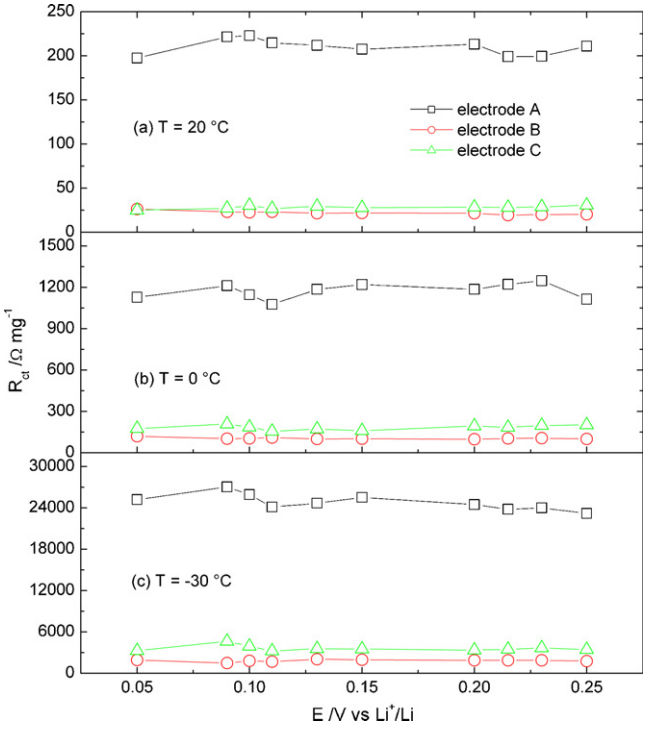

Fig. 9. Values of charge-transfer resistances for electrodes A–C at 20 °C (panel a), 0 °C (panel b), −30 °C (panel c) as a function of potential.

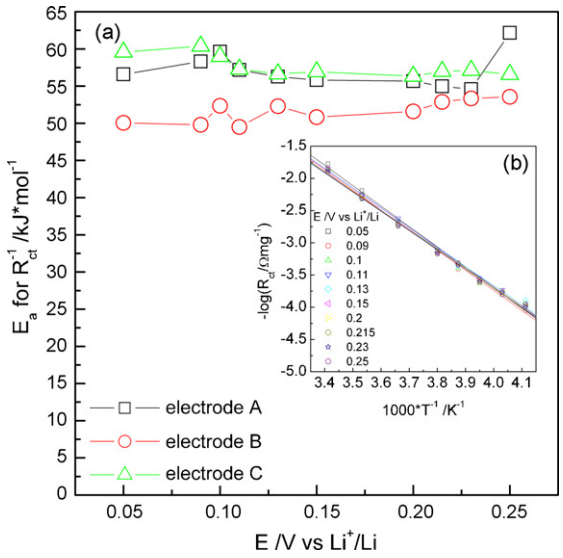

Fig. 10. (a) Trends of activation energy for the charge-transfer process as calculated by Arrhenius plots, shown in detail in panel (b) for electrode B.

A, E_a and R represent, respectively a pre-exponential factor, the activation energy for the charge-transfer process and the universal constant of gases. The obtained values for E_a, and the corresponding Arrhenius plots of the R_{ct} for electrode B, are shown in Fig. 10, panel (a) and (b), respectively.

The average values allover the entire potential range are about 57 kJ mol^{-1} for electrode A, 51 kJ mol^{-1} for electrode B and 57 kJ mol^{-1} for electrode C.

The Sn-coated electrode B benefits of the catalytic effect at every potential, since the activation energy values for the charge-transfer process are 6 kJ mol^{-1} lower than those found for the pristine oxidized graphite electrode A. This reduction is in agreement with that already observed for Cu–graphite composites [27]. The activation energies are consistent with the values listed by Ogumi and Xu [40–43] for a process limited by the desolvation rate, as demonstrated by a study of the break-up of a Li^+ ion solvation shell formed by several organic solvents, that resulted in activation energies for charge-transfer depending both on the strength of coordination of intercalating Li^+ ion and on the chemistry of interface. We can assume that Sn coating of electrode B affects both strength of Li^+/solvent interactions and SEI chemistry, as already revealed by reduced SEI resistance and increased irreversible capacity at the first cycle.

It should be pointed out that Li^+ ion migration through the surface Sn layer does not follow the same mechanism hypothesized in the case of a non-alloy forming metal as Cu. In fact, while the mass transfer of the Li^+ ion through a compact Cu layer can occur only through the vacant spaces occasionally created by lattice defects or phonon vibrations [29,53], the migration through the Sn layer is most likely occurring through alloying/dealloying processes. However, migration through the metallic layers, either in the case of Cu or Sn, requires the complete desolvation of the adion at the electrode/electrolyte interface. The macroscopic effect, i.e. the reduction of the related activation energy, is thus comparable for Sn- and Cu-coated electrodes.

For electrode C, containing Sn nanopowder dispersed in the bulk of graphite, the activation energy values are comparable to those of electrode A. This is probably due to the fact that the finely dispersed Sn may act only locally rather than constituting a physical barrier over the entire electrode surface.

Nevertheless, also the electrode C shows higher reversible capacities at low temperatures and a lower polarization than electrode A. In addition, the reduced R_{ct} values observed in Fig. 9 leave no doubts about an active role exerted by Sn powder in enhancing the charge-transfer rate. This behavior can be explained by a bulk effect produced by the finely dispersed Sn powder. The overall charge-transfer process involves both solvated Li^+ ions, that approach the interface from electrolyte side, and electrons from current collector side in order to restore electroneutrality. The main contribution of the dispersed Sn powder is thus probably an improvement of the bulk conductivity of the electrodes, that enhances the inter-particles electron conduction, together with a local effect on the intercalation mechanism.

4. Conclusions

Sn–graphite composite anodes containing very low amounts of metal, either as a nanopowder dispersed in the bulk or as a surface layer, show good cycling stability and great performances improvements at low temperatures with respect to unmodified graphite electrodes. The analysis of intercalation kinetics, performed by cyclic voltammetry and electrochemical impedance spectroscopy, reveals an improvement in the rate of charge-transfer process, that can been mainly attributed to a catalysis of adion desolvation by the surface Sn coating, or to an enhancement of internal conductivity of the bulk electrode by the Sn dispersed powder. A further contribution evidenced by both kinds of Sn–graphite composites is an increase of passivation layer conductivity, probably due to the incorporation of part of the metal into the SEI. This behavior makes this class of electrodes particularly appealing for low-temperature operation.

With the aim to validate the proposed kinetic models, further studies are currently in progress involving Sn–graphite composites with different formulations, e.g. containing different amounts of dispersed Sn or coated by metallic layers of different thicknesses.

Acknowledgment

This work was supported by MIUR, PRIN 2007.

References

[1] C.K. Huang, J.S. Sakamoto, J. Wolfenstine, S. Surampudi, J. Electrochem. Soc. 147 (2000) 2893.
[2] S.S. Zhang, K. Xu, T.R. Jow, Electrochim. Acta 48 (2002) 241.
[3] H.P. Lin, D. Chua, M. Salomon, H.C. Shiao, M. Hendrickson, E. Plichta, S. Slane, Electrochem. Solid-State Lett. 4 (2001) A71.
[4] G. Nagasubramanian, J. Appl. Electrochem. 31 (2001) 99.
[5] F. Nobili, S. Dsoke, T. Mecozzi, R. Marassi, Electrochim. Acta 51 (2005) 536.
[6] E. Peled, C. Menachem, D. Bar-Tow, A. Melman, J. Electrochem. Soc. 143 (1996) L4.
[7] S.S. Zhang, K. Xu, T.R. Jow, J. Solid State Electrochem. 7 (2003) 147.
[8] S.S. Zhang, K. Xu, T.R. Jow, Electrochem. Commun. 4 (2002) 928.
[9] E.J. Plichta, M. Hendrickson, R. Thompson, G. Au, W.K. Behl, M.C. Smart, B.V. Ratnakumar, S. Surampudi, J. Power Sources 94 (2001) 160.
[10] M.C. Smart, B.V. Ratnakumar, S. Surampudi, J. Electrochem. Soc. 149 (2002) A361.
[11] S. Takeuchi, H. Honbo, Y. Muranaka, S. Yamauchi, M. Yoshikawa, US Patent no. 6,030,726 (2000).
[12] P. Yu, J.A. Ritter, R.E. White, B.N. Popov, J. Electrochem. Soc. 147 (2000) 1280.
[13] P. Yu, J.A. Ritter, R.E. White, B.N. Popov, J. Electrochem. Soc. 147 (2000) 2081.
[14] J.Y. Lee, R. Zhang, Z. Liu, J. Power Sources 90 (2000) 70.
[15] B. Veeraraghavan, A. Durairajan, B. Haran, B. Popov, R. Guidotti, J. Electrochem. Soc. 149 (2002) 675.
[16] H. Huang, E.M. Kelder, J. Schoonman, J. Power Sources 97/98 (2001) 114.
[17] Z. Liu, A. Yu, J.H. Lee, J. Power Sources 81/82 (1999) 187.
[18] T. Takamura, K. Sumiya, J. Suzuki, C. Yamada, K. Sekine, J. Power Sources 81/82 (1999) 368.
[19] K. Sumiya, J. Suzuki, R. Takasu, K. Sekine, T. Takamura, J. Electroanal. Chem. 462 (1999) 150.
[20] T. Takamura, J. Suzuki, C. Yamada, K. Sumiya, K. Sekine, Surf. Eng. 15 (1999) 225.
[21] J. Suzuki, M. Yoshida, Y. Nishijima, K. Sekine, T. Takamura, Electrochim. Acta 47 (2002) 3881.
[22] H. Momose, H. Honbo, S. Takeuchi, K. Nishimura, T. Horiba, Y. Muranaka, Y. Kozono, H. Miyadera, J. Power Sources 68 (1997) 208.

[23] L. Shi, Q. Wang, H. Li, Z. Wang, X. Huang, L. Chen, J. Power Sources 102 (2001) 60.
[24] G. Nadeau, X. Yun Song, M. Massé, A. Guerfi, G. Brisard, K. Kinoshita, K. Zaghib, J. Power Sources 108 (2002) 86.
[25] Y.P. Wu, C. Jiang, R. Holze, J. Power Sources 112 (2002) 255.
[26] S.S. Kim, Y. Kadoma, H. Ikuta, Y. Uchimoto, M. Wakihara, Electrochem, Solid State Lett. 4 (2001) 109.
[27] M. Mancini, F. Nobili, S. Dsoke, F. D'Amico, R. Tossici, F. Croce, R. Marassi, J. Power Sources 190 (2009) 141.
[28] F. Nobili, S. Dsoke, M. Mancini, R. Tossici, R. Marassi, J. Power Sources 180 (2008) 845.
[29] F. Nobili, S. Dsoke, M. Mancini, R. Marassi, Fuel Cells 9 (2009) 264.
[30] G. Derrien, J. Hassoun, S. Panero, B. Scrosati, Adv. Mater. 19 (2007) 2336.
[31] J. Hassoun, G. Derrien, S. Panero, B. Scrosati, Adv. Mater. 20 (2008) 3169.
[32] I. Grigoriants, L. Sominski, H. Li, I. Ifargan, D. Aurbach, A. Gedanken, Chem. Commun. (2005) 921.
[33] Y. Wang, J.-Y. Lee, J. Power Sources 144 (2005) 220.
[34] B. Guo, J. Shu, K. Tang, Y. Bai, Z. Wang, L. Chen, J. Power Sources 177 (2008) 205.
[35] Z.P. Guo, E. Milin, J.Z. Wang, J. Chen, H.K. Liua, J. Electrochem. Soc. 152 (2005) A2211.
[36] M.K. Datta, P.N. Kumta, J. Power Sources 194 (2009) 1043.
[37] G.X. Wang, J.H. Ahn, J. Yao, H.K. Liu, Electrochem. Commun. 6 (2004) 689.
[38] M. Mancini, P. Kubiak, J. Geserick, R. Marassi, N. Hüsing, M. Wohlfahrt-Mehrens, J. Power Sources 189 (2009) 585–589.
[39] M. Mancini, P. Kubiak, M. Wohlfahrt-Mehrens, R. Marassi, J. Electrochem. Soc. 157 (2010) A164.
[40] K. Xu, Y. Lam, S.S. Zhang, T.R. Jow, T.B. Curtis, J. Phys. Chem. C 111 (2007) 7411.
[41] K. Xu, J. Electrochem. Soc. 154 (2007) A162.
[42] T. Abe, H. Fukuda, Y. Iriyama, Z. Ogumi, J. Electrochem. Soc. 151 (2004) A1120.
[43] T. Abe, F. Sagane, M. Ohtsuka, Y. Iriyama, Z. Ogumi, J. Electrochem. Soc. 152 (2005) A2151.
[44] H.C. Shiao, D. Chua, H.P. Ling, S. Slane, M. Salomon, J. Power Sources 87 (2000) 167.
[45] J. Hassoun, P. Reale, S. Panero, J. Power Sources 174 (2007) 321.
[46] E. Barsoukov, J. Ross Macdonald, Impedance Spectroscopy. Theory, Experiments and Applications, second ed., John Wiley & Sons, New York, 2005, p. 27.
[47] P.G. Bruce, M.Y. Saidi, J. Electroanal. Chem. 322 (1992) 93.
[48] F. Croce, F. Nobili, A. Deptula, W. Lada, R. Tossici, A. D'Epifanio, B. Scrosati, R. Marassi, Electrochem. Commun. 1 (1999) 605.
[49] F. Nobili, R. Tossici, F. Croce, B. Scrosati, R. Marassi, J. Power Sources 94 (2001) 238.
[50] F. Nobili, R. Tossici, R. Marassi, F. Croce, B. Scrosati, J. Phys. Chem. B 106 (2002) 3909.
[51] B.A. Boukamp, Solid State Ionics 20 (1986) 159.
[52] E. Barsoukov, J. Ross Macdonald, Impedance Spectroscopy. Theory, Experiments and Applications, second ed., John Wiley & Sons, New York, 2005, p. 83.
[53] J. Suzuki, M. Yoshida, C. Nakahara, K. Sekine, M. Kikuchi, T. Takamura, Electrochem. Solid-State Lett. 4 (2001) A1.
[54] F. Nobili, M. Mancini, S. Dsoke, R. Tossici, R. Marassi, in preparation.